frontiers | Frontiers in Physics

ORIGINAL RESEARCH
published: 08 August 2022
doi: 10.3389/fphy.2022.929033

Porous Silicon–Based Microring Resonator for Temperature and Cancer Cell Detection

Rahul Kumar Gangwar[1], Jun Qin[2] and Xingjun Wang[1,3]**

[1]State Key Laboratory of Advanced Optical Communication Systems and Networks, School of Electronics, Peking University, Beijing, China, [2]School of Information and Communication Engineering, Beijing Information Science and Technology University, Beijing, China, [3]Nano-optoelectronics Frontier Center of Ministry of Education, Peking University, Beijing, China

In this article, a microring resonator sensor based on porous silicon is proposed for temperature and cancer cell detection, simultaneously. The porous behavior of silicon with a large internal surface area allows external materials to interact directly with the guided modes. The resonance wavelength in the transmission spectrum of the microring resonator is very sensitive to external environmental properties such as refractive index and temperature. The transmission characteristics of the proposed sensor were numerically determined by full vectorial finite element analysis. The achieved maximum sensitivity of the proposed sensor with optimized parameters was 150 pm/°C for an operational temperature range of 20–100°C and 284.0306 nm/RIU for operational cancer cell detection, respectively. The results presented here suggest the microring resonator sensor can be used in the fields of environment sensing, temperature sensing, chemical sensing, and biosensing.

Keywords: cancer cell detection, optical sensors, optical resonators, refractive index sensor, temperature sensors

Edited by:
Sushank Chaudhary, Quanzhou Institute of Equipment manufacturing (CAS), China

Reviewed by:
Sneha Kumari, Indian Institute of Technology Patna, India
Dharmendra Kumar, Madan Mohan Malaviya University of Technology, India

****Correspondence:***
Rahul Kumar Gangwar
rahul0889@gmail.com
Xingjun Wang
xjwang@pku.edu.cn

Specialty section:
This article was submitted to Optics and Photonics, a section of the journal Frontiers in Physics

Received: *26 April 2022*
Accepted: *05 May 2022*
Published: *08 August 2022*

Citation:
Gangwar RK, Qin J and Wang X (2022) Porous Silicon–Based Microring Resonator for Temperature and Cancer Cell Detection. Front. Phys. 10:929033. doi: 10.3389/fphy.2022.929033

INTRODUCTION

The development of optical sensors to detect various biomolecules, viruses, and traces of hazardous gases is very important. Different kinds of optical sensors such as evanescent waveguides, Mach-Zehnder interferometers, optical fibers, slot waveguides, photonic crystals, and microring resonator–based sensors have been developed for the fast, sensitive, and selective detection of physical and chemical parameters in a surrounding medium [1–16]. Among various kinds of optical sensors, optical microring resonators (MRR) are probably the most often used photonic integrated structures used as a sensing device due to their high sensitivity, compact size, fast and accurate response, and structural simplicity [17–19]. Most of the MRR-based sensors are based on the evanescent wave detection method. The electromagnetic wave that propagates in the waveguide is accompanied by an evanescent wave that extends outside the ring and thus directly interacts with the surrounding analyte. This interaction is sensitive to changes in the refractive index (RI) of the analyte or temperature, resulting in a wavelength shift in the output spectrum of the device. This shift in wavelength can be used to detect anything that affects the optical properties of the MRR, for example, temperature or refractive index changes in the surrounding medium [20, 21]. In a practical optical sensing environment, both RI and temperature have a large effect on the wavelength shift of the transmission spectrum of the device. To date, different types of optical sensors have been established for dual parameter sensing. Shi et al. proposed a photonic crystal (PhC) sensor of two PhC nanobeam cavities as a dual parameter sensor with a refractive

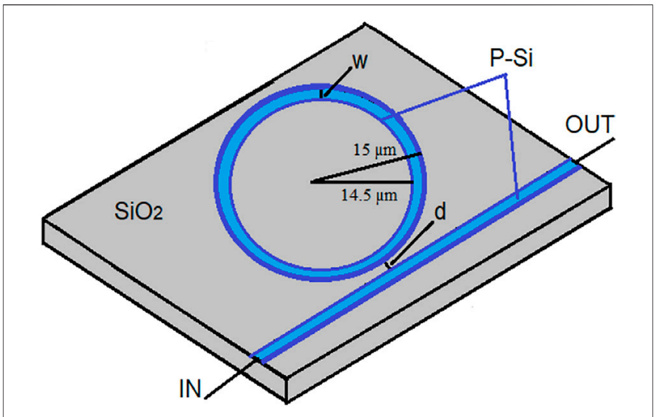

FIGURE 1 | Cross-section of the proposed microring resonator–based temperature sensor.

index sensitivity of 256.4 nm/RIU and temperature sensitivity of 30.1 pm/K, simultaneously [22]. However, the performances of these high-refractive index contrast-based planner photonic sensing devices are limited because most of the distribution of the optical field, associated with the guided mode, is propagated inside the waveguide itself.

To overcome these limitations and to enhance light-analyte interactions to improve its sensing capabilities, porous materials such as porous silicon (P-Si) have been used for MRR-based sensing devices [23–28]. Micro and nanostructured silicon is a three-dimensional porous material used to enhance molecular interactions with the guided electromagnetic fields. Because of the high specific internal surface, the number of binding sites for surface functionalization is increased, which enhances the light-analyte interactions and provides better sensing performance. Moreover, P-Si can be easily formed by the inexpensive electrochemical etching of a silicon substrate [29]. Rodriguez et al. first presented a P-Si-based MRR sensor for saltwater measurement with a sensitivity of 380 nm/RIU [30]. P-Si is very attractive because of its ultra-high internal surface and it is characterized by a very high surface-to-volume ratio. This allows the immobilization of a large amount of bioreceptors over the inner walls of the pores for the better detection of target biomolecules.

In this study, we present a P-Si MRR structure for the detection of temperature and various cancer cell types with a specific refractive index, simultaneously. By using the finite element method, we optimized the structural parameters of the structure and characterized the transmission response. Sensing performance against different temperatures and cancer cells was obtained simultaneously by measuring the wavelength shifts in the transmission spectrum of the MRR. P-Si was chosen in this study because of its large internal surface area, large surface functionalization chemistry, large achievable RI contrast between adjacent layers, and low cost compared with SOI. P-Si films can achieve a very large surface area of about 180 m^2/cm^3, which leads to improved sensor performance [31].

THEORETICAL MODEL AND ANALYSIS

The proposed sensing device for temperature and refractive index detection is shown in **Figure 1**. The P-Si ring and bus waveguide were placed on a thick silica substrate (n = 1.45). The outer and inner radii of the ring were 15 and 14.5 µm, respectively. The width of the waveguide is denoted by "w" and the distance between the bus waveguide and ring is denoted by "d."

The refractive index and porosity of silicon material were obtained by the following equation [32]:

$$(1-p).\frac{n_s^2-n_{ps}^2}{n_s^2+2n_{ps}^2}+(p-V).\frac{n_a^2-n_{ps}^2}{n_a^2+2n_{ps}^2}+V.\frac{n_d^2-n_{ps}^2}{n_d^2+2n_{ps}^2}=0 \quad (1)$$

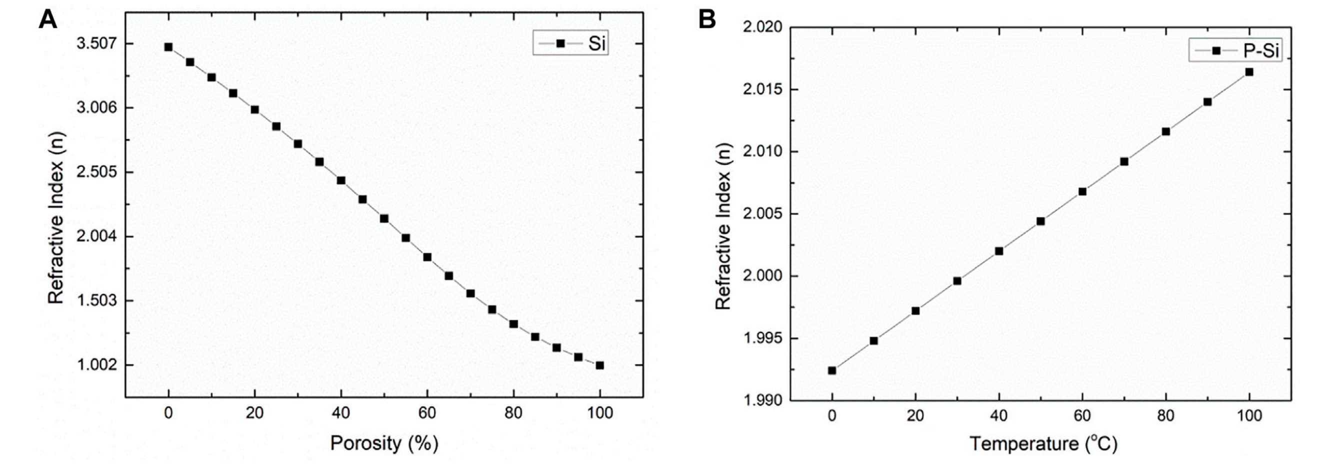

FIGURE 2 | (A) Variations in the refractive index with porosity for silicon material and **(B)** variations in the refractive index with temperature for the porous silicon material.

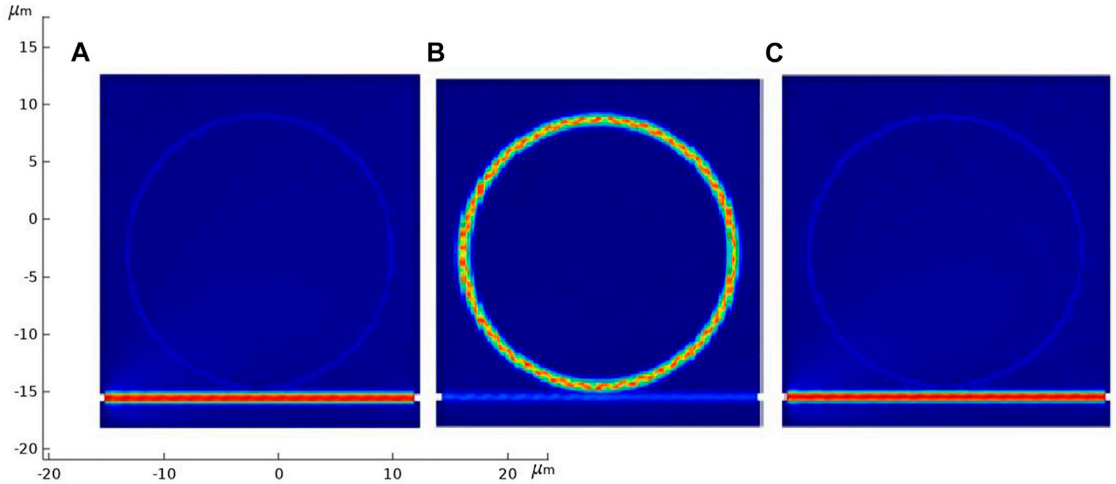

FIGURE 3 | Electric field distribution when the temperature is fixed at 30°C, and when the wavelength is **(A)** 1,542 nm, **(B)** 1,546 nm, or **(C)** 1,550 nm.

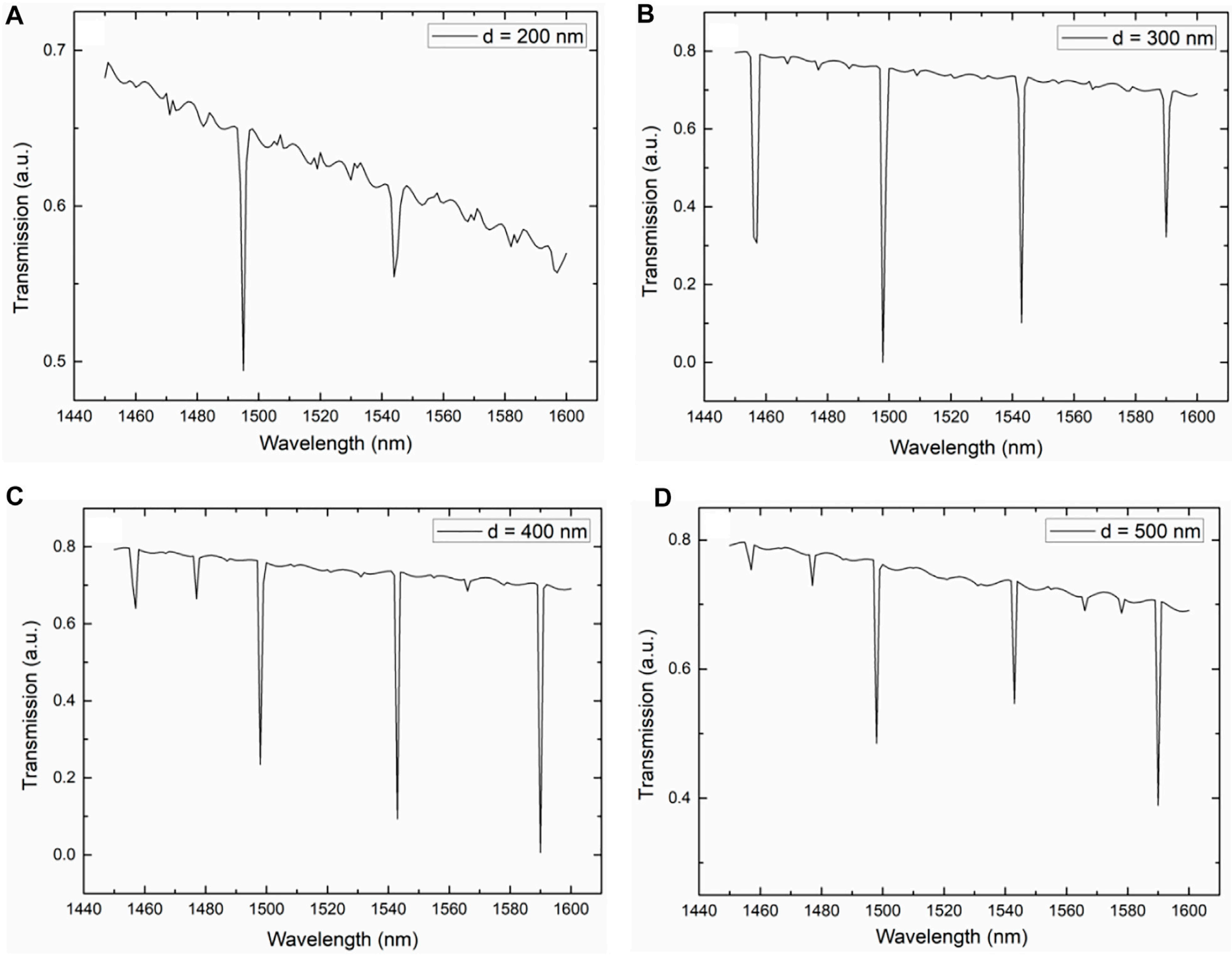

FIGURE 4 | Transmission curve of the device for different distances between the ring and bus waveguide varying from 200 to 500 nm by 100 nm.

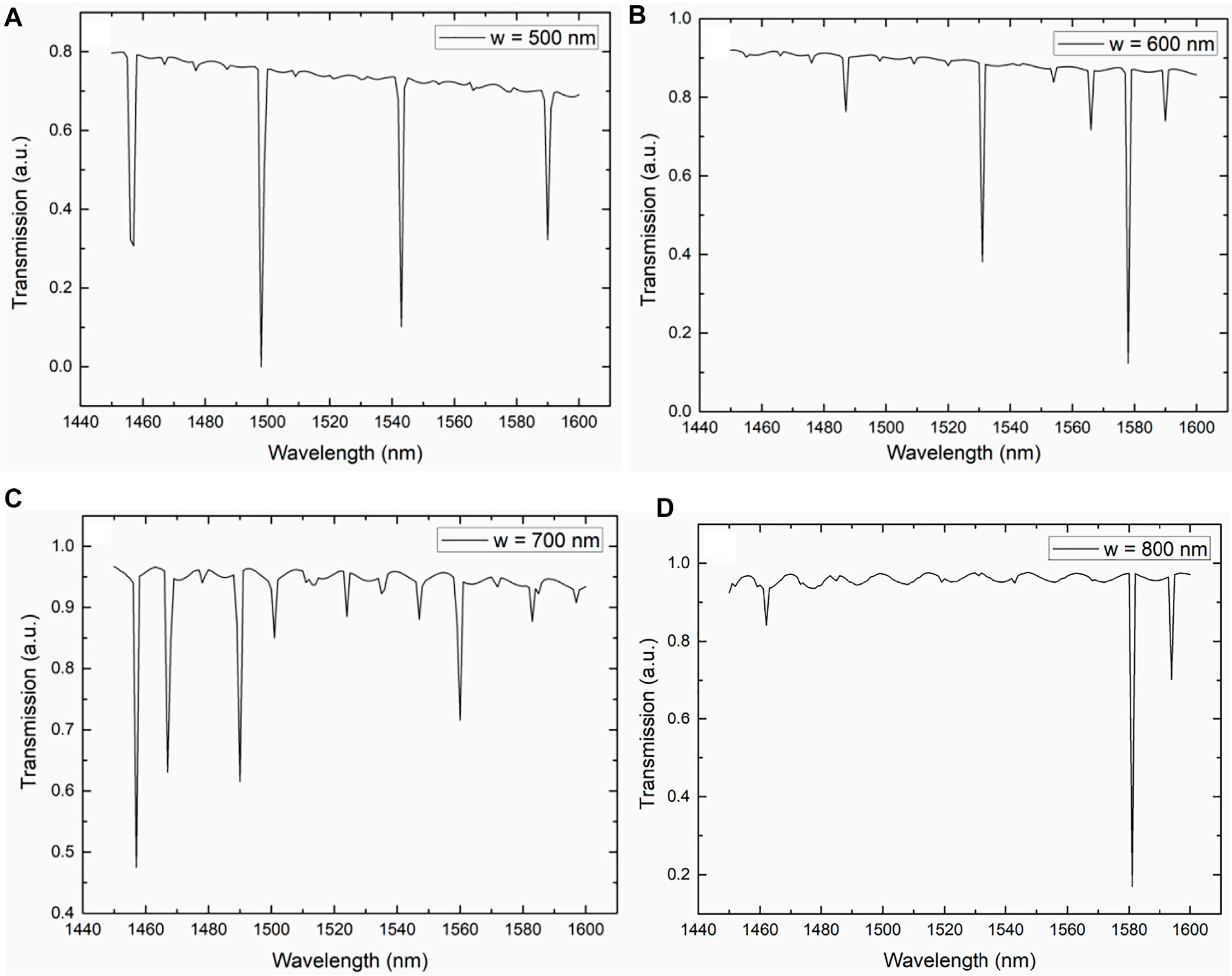

FIGURE 5 | Transmission curve of the sensor for different widths of the ring and waveguide varying from 500 to 800 nm by 100 nm.

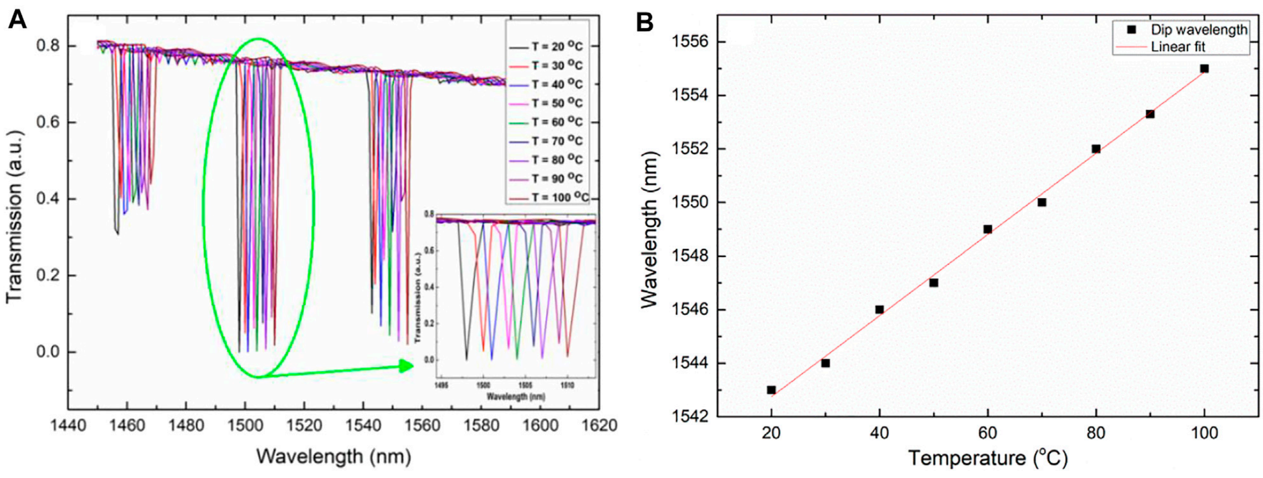

FIGURE 6 | (A) Transmission spectra of the sensor with 55% porosity at different temperatures varying from 20 to 100°C. The inset shows the enlarged view of the transmission spectrum near the 1,505 nm wavelength. **(B)** Variations in the dip wavelength around 1,550 nm with different temperatures.

TABLE 1 | Different cancer cells and their corresponding RI.

Cancer Cells name	Cell types	Refractive index
Jurkat	Blood Cancer	1.390
HeLa	Cervical Cancer	1.392
PC12	Adrenal Gland Cancer	1.395
MDA-MB-231	Breast Cancer	1.399
MCF-7	Breast Cancer	1.401
Basal	Skin Cancer	1.380

where p is the porosity, n_s is the refractive index of silicon, n_{ps} is the refractive index of porous silicon, n_a is the refractive index of air, n_d is the refractive index of the analyte filled in pores, and V is the volume fraction of the pores. The porosity of P-Si is 55%, and the corresponding refractive index of P-Si is 1.9924.

For temperature sensing, the temperature-dependent refractive index of the material was obtained from the following equation [33]:

$$n = n_0 + \alpha(T - T_0) \tag{2}$$

where n_0 is the refractive index of the medium, α is the thermo-optic coefficient of P-Si, T is the final temperature, and T_0 is the initial temperature.

Figure 2A shows the variation in the refractive index of silicon with different porosities, and **Figure 2B** presents the refractive index of P-Si at different temperatures.

The MRR intensity transmission was obtained by the following equation:

$$T(\lambda) = \left|\frac{E_t}{E_i}\right|^2 \tag{3}$$

where E_t and E_i are the field amplitudes of the incoming and transmitted waves. At the output end of the waveguide, resonance occurs in the transmission spectrum at λ_{res} according to the following equation:

$$\lambda_{res} = 2\pi L n_{eff} \big/ p \tag{4}$$

where "L" is the perimeter of MRR, "n_{eff}" is the effective refractive index of the guided mode, and "p" is an integer parameter.

The proposed sensor was simulated in two dimensions with full vectorial finite element–based COMSOL Multiphysics software. During the simulation, the cross-section of the proposed sensor structure was divided into very small parts or meshes. To absorb light radiating towards the surface, perfectly matched layer boundary conditions were used. Simulation analysis was performed in the XY-plane and light was propagated in the Z-direction. Then, a free triangular mesh with an extremely fine mesh size containing 27,402 domain elements and 1,456 boundary elements was considered for the characterization of the proposed sensor and 192,617 degrees of freedom were solved during the simulation process.

The electric field distribution of the fundamental guided mode at different wavelengths with a fixed temperature (30°C) is shown in **Figure 3**. Here, we observed that light was well confined in the bus and ring waveguide. Also, coupling between the bus waveguide and ring waveguide occurred as shown in **Figure 3B** obtained from the simulation.

RESULTS AND DISCUSSION

Light entered one end of the bus waveguide and was coupled into the ring by evanescent coupling. The transmission spectrum of the structure was obtained at the other end of the bus waveguide. **Figure 4** shows the transmission spectrum of the sensor at different distances "d" between the ring and waveguide when the RI of the sensing analyte was set as 1, that is, air at room temperature. The values of "d" varied from 200 to 500 nm at a gap of 100 nm. From these simulation results, we can see that when d = 300 nm, the transmission spectrum of the device was regular compared with the other samples. From these simulation results, we obtained an optimized value of "d" that was used for the rest of our studies because it had less distortion in the transmission spectrum, which is useful for the sensing analysis.

After obtaining the optimized value of "d," we considered the effect of the width "w" of the ring and waveguide on the transmission properties of the structure. **Figure 5** shows the obtained transmission spectrum of the structure at fixed "d" with different values of the waveguide and ring width "w," which varied from 500 to 800 nm by 100 nm. **Figure 5A** represents the simulated transmission spectrum when "w" was set at 500 nm, which had four clear dips in the transmission spectra compared with the other values. This helps to measure the shift in the transmission spectrum when the device is subjected to variations in the surrounding parameters, in our case, temperature and refractive index, which have an impact on the transmission spectrum.

Using the optimized structural parameters, the present structure was used for temperature and refractive index detection. We changed the temperature of the surrounding environment from 20 to 100°C by 10°C. **Figure 6A** shows the simulated results of the variation in the transmission spectrum of the sensor at different temperatures. The inset of **Figure 6A**shows an enlarged view of the transmission spectrum near 1,505 nm in which the corresponding dips in the transmission spectrum clearly shifts with the changes in temperature. There was a red shift in the transmission spectrum. **Figure 6B** depicts the simulation results of the variation in the dip wavelength around 1,505 nm with different temperatures. The dip wavelength shifted towards a higher wavelength as the temperature increased. The maximum sensitivity of the sensors subjected to temperature changes was 0.1515 nm/°C (151.5 pm/°C) for the temperature range 20–100°C with a linearity of 0.99623, which is better than previously published data [33–38]. Here, the light-matter interaction inside the pores was increased and because of this

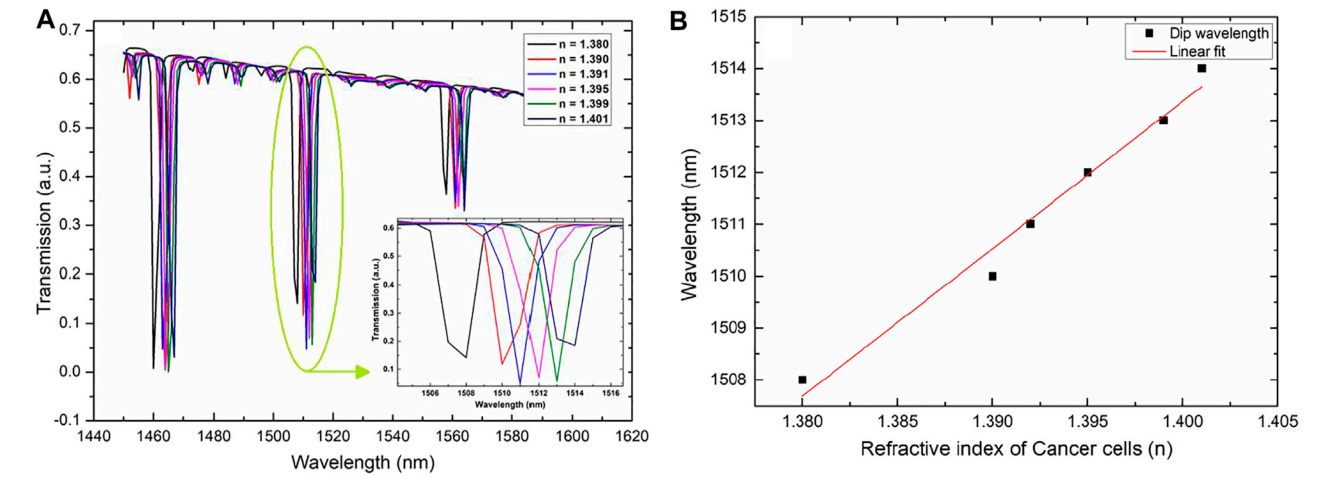

FIGURE 7 | (A) Transmission spectra of the sensor with 55% porosity at different refractive indexes of cancer cells varying from 1.380 to 1.401. The inset shows an enlarged view of the transmission spectrum near the 1,510 nm wavelength. **(B)** Variations in the dip wavelength at different refractive indexes near 1,550 nm.

increased interaction, we obtained high sensitivity and good performance of the proposed sensor.

Next, the present sensor was tested for RI sensing. Here, we chose values of RI corresponding to different cancer cells whose refractive indexes vary between 1.380 and 1.401. **Table 1** shows the refractive indexes of the different cancer cells [39].

Figure 7A presents the obtained transmission spectra by the simulation of the proposed sensor when the RI of the surrounding medium was changed from 1.380 to1.401, related to the different cancer cells. When the RI of the target cells changed towards a higher value, the dip wavelength in the transmission spectrum changed from a lower wavelength to a higher wavelength; that is, a red shift occurred. We observed a shift in the dip wavelength corresponding to the different cancer cells in the inset of **Figure 7A**. The dip wavelengths of the transmission spectra for different target cancer cells and their corresponding RI are plotted in **Figure 7B** as obtained from the simulation results. By taking the slope of the plot, we obtained the sensitivity of the proposed sensor for cancer cell detection, which was approximately 284.0306 nm/RIU with a linearity of 0.97235. This high sensitivity value with very good linearity was achieved because of the porous nature of the ring that allowed the sensing material to be injected into the large volume inside the ring where most of the optical power is confined.

The present sensors can be realized experimentally in which a broadband source and optical spectrum analyzer are used. Light of different wavelengths from the broadband source will land on one end of the sensor bus waveguide with the help of conventional fibers and will then be collected by the optical spectrum analyzer at the other end. The sensing portion will be immersed in liquids with different refractive indices and the transmission characteristics of each will be observed. Shifts in the transmission spectrum will be used to determine the sensitivity of the proposed sensor.

Recently, the fabrication of a porous silicon–based microring resonator was reported by Rodriguez et al. [30]. First, the fabrication of P-Si slab waveguides was achieved by electrochemical etching. Then, a guiding layer was created by applying a current. Next, a cladding layer was etched, the samples were oxidized, and the resulting waveguides were fabricated. Rings were patterned on the fabricated waveguide using the reactive ion etching standard and electron beam lithography. Finally, different ring sizes rings were drawn. A short oxidation step was performed for the smooth sidewalls of the patterned P-Si ring resonator.

CONCLUSION

In conclusion, a P-Si-based MRR sensor was developed for the simultaneous sensing of different temperatures and detection of cancer cells. The sensing performance of the devices was characterized using the finite element method. The effects of various structural parameters were also investigated. Numerical results show the temperature sensitivity was 150 pm/°C for a temperature range of 20–100°C with a linearity of 0.99532 and RI sensitivity corresponding to the different cancer cells of 284.0306 nm/RIU. The enormous internal surface area of P-Si and its accompanying high light-matter interactions between the guided mode and target molecules in the pores give P-Si ring resonators a greater sensing capability than ordinary ring resonators. The proposed sensor has potential applications in the field of biosensing and the detection of multiparameters such as RI, temperature, and humidity.

DATA AVAILABILITY STATEMENT

The raw data supporting the conclusion of this article will be made available by the authors, without undue reservation.

AUTHOR CONTRIBUTIONS

RG: methodology, conceptualization, formal analysis, validation, funding acquisition, and writing—original draft. JQ: formal analysis, validation, and writing—review and editing. XW: conceptualization, formal analysis, validation, funding acquisition, supervision, and writing—review and editing.

FUNDING

This work was supported in part by the National Natural Science Foundation of China under Grant No. 62001010, National Key R&D Program of China under Grant No. 2021YFB2800400, and the Beijing Natural Science Foundation under Grant No. Z210004.

REFERENCES

1. Estevez MC, Alvarez M, Lechuga LM. Integrated Optical Devices for Lab-on-A-Chip Biosensing Applications. *Laser Photon Rev* (2012) 6(4):463–487. doi:10.1002/lpor.201100025
2. Azizi B, Shabankareh MAG, Farmani A. Simulation of a Refractive index Sensor Based on the Vernier Effect and a Cascaded PANDA and Mach-Zehnder Interferometer. *J Comput Electron* (2021) 20:1599–1610. doi:10.1007/s10825-021-01726-3
3. Pan Q, Luo X. A 58-dBΩ 20-Gb/s Inverter-Based Cascode Transimpedance Amplifier for Optical Communications. *J Semicond* (2022) 43(1):012401. doi:10.1088/1674-4926/43/1/012401
4. Kozma P, Kehl F, Ehrentreich-Förster E, Stamm C, Bier FF. Integrated Planar Optical Waveguide Interferometer Biosensors: A Comparative Review. *Biosens Bioelectron* (2014) 58:287–307. doi:10.1016/j.bios.2014.02.049
5. Omidniaee A, Karimi S, Farmani A. Surface Plasmon Resonance-Based SiO_2 Kretschmann Configuration Biosensor for the Detection of Blood Glucose. *Silicon* (2022) 14:3081–3090. doi:10.1007/s12633-021-01081-9
6. Shen B, Shu H, Zhou L, Wang X. A Design Method for High Fabrication Tolerance Integrated Optical Mode Multiplexer. *Sci China Inf Sci* (2020) 63(6): 160409. doi:10.1007/s11432-020-2888-2
7. Bai B, Shu H, Wang X, Zou W. Towards Silicon Photonic Neural Networks for Artificial Intelligence. *Sci China Inf Sci* (2020) 63(6):160403. doi:10.1007/s11432-020-2872-3
8. Farmani H, Farmani A, Biglari Z. A Label-free Graphene-Based Nanosensor Using Surface Plasmon Resonance for Biomaterials Detection. *Phys. E: Low-Dimens. Syst. Nanostructures* (2020) 116:113730. doi:10.1016/j.physe.2019.113730
9. Chiang L-Y, Wang C-T, Lin T-S, Pappert S, Yu P. Highly Sensitive Silicon Photonic Temperature Sensor Based on Liquid crystal Filled Slot Waveguide Directional Coupler. *Opt Express* (2020) 28(20):29345–29456. doi:10.1364/oe.403710
10. Liu Q, Tu X, Kim KW, Kee JS, Shin Y, Han K, et al. Highly Sensitive Mach-Zehnder Interferometer Biosensor Based on Silicon Nitride Slot Waveguide. *Sens Actuators B Chem* (2013) 188:681–688. doi:10.1016/j.snb.2013.07.053
11. Khosravian E, Mashayekhi HR, Farmani A. Highly Polarization-Sensitive, Broadband, Low Dark Current, High Responsivity Graphene-Based Photodetector Utilizing a Metal Nano-Grating at Telecommunication Wavelengths. *J Opt Soc Am B* (2021) 38(4):1192–1199. doi:10.1364/josab.418804
12. Gangwar RK, Amorim VA, Marques PVS. High Performance Titanium Oxide Coated D-Shaped Optical Fiber Plasmonic Sensor. *IEEE Sensors J* (2019) 19(20):9244–9248. doi:10.1109/jsen.2019.2927728
13. Pathak AK, Singh VK. SPR Based Optical Fiber Refractive Index Sensor Using Silver Nanowire Assisted CSMFC. *IEEE Photon Technol Lett* (2020) 32(8): 465–468. doi:10.1109/lpt.2020.2980470
14. Chakravarty S, Chen X, Tang N, Lai W, Yan H, Chen RT. Review of Design Principles of 2D Photonic Crystal Microcavity Biosensors in Silicon and Their Applications. *Front Optoelectron* (2016) 9(2):206–224. doi:10.1007/s12200-016-0631-2
15. Kaur B, Kumar S, Kaushik BK. 2D Materials-Based Fiber Optic SPR Biosensor for Cancer Detection at 1550 nm. *IEEE Sensors J* (2021) 21(21):23957–23964. doi:10.1109/jsen.2021.3110967
16. Kaur B, Kumar S, Kaushik BK. MXenes-Based Fiber-Optic SPR Sensor for Colorectal Cancer Diagnosis. *IEEE Sensors J* (2022) 22(7):6661–6668. doi:10.1109/jsen.2022.3154385
17. Amoosoltani N, Mehrabi K, Zarifkar A, Farmani A, Yasrebi N. Double-Ring Resonator Plasmonic Refractive Index Sensor Utilizing Dual-Band Unidirectional Reflectionless Propagation Effect. *Plasmonics* (2021) 16: 1277–1285. doi:10.1007/s11468-021-01395-9
18. Amoomoosoltani N, yasrebi N, Farmani A, Zarifkar A. A Plasmonic Nano-Biosensor Based on Two Consecutive Disk Resonators and Unidirectional Reflectionless Propagation Effect. *IEEE Sensors J* (2020) 20(16):9097–9104. doi:10.1109/jsen.2020.2987319
19. Washburn AL, Gunn LC, Bailey RC. Label-Free Quantitation of a Cancer Biomarker in Complex media Using Silicon Photonic Microring Resonators. *Anal Chem* (2009) 81(22):9499–9506. doi:10.1021/ac902006p
20. Steglich P, Hülsemann M, Dietzel B, Mai A. Optical Biosensors Based on Silicon-On-Insulator Ring Resonators: A Review. *Molecules* (2019) 24(3):519. doi:10.3390/molecules24030519
21. Bogaerts W, De Heyn P, Van Vaerenbergh T, De Vos K, Selvaraja SK, Claes T, et al. Silicon Microring Resonators. *Laser Photon Rev* (2012) 6(1):47–73. doi:10.1002/lpor.201100017
22. Liu P, Shi Y. Simultaneous Measurement of Refractive index and Temperature Using Cascaded Side-Coupled Photonic crystal Nanobeam Cavities. *Opt Express* (2017) 25(23):28398–28406. doi:10.1364/oe.25.028398
23. Dhanekar S, Jain S. Porous Silicon Biosensor: Current Status. *Biosens Bioelectron* (2013) 4(1):54–64. doi:10.1016/j.bios.2012.09.045
24. Harraz FA. Porous Silicon Chemical Sensors and Biosensors: A Review. *Sens Actuators B Chem* (2014) 202:897–912. doi:10.1016/j.snb.2014.06.048
25. Zhang H, Jia Z, Lv X, Zhou J, Chen L, Liu R, et al. Porous Silicon Optical Microcavity Biosensor on Silicon-on-Insulator Wafer for Sensitive DNA Detection. *Biosens Bioelectron* (2013) 44:89–94. doi:10.1016/j.bios.2013.01.012
26. Baratto C, Faglia G, Comini E, Sberveglieri G, Taroni A, Ferrara V, et al. A Novel Porous Silicon Sensor for Detection of Sub-ppm NO2 Concentrations. *Sens Actuators B Chem* (2001) 77(1–2):62–66. doi:10.1016/s0925-4005(01)00673-6
27. Kim K, Murphy TE. Porous Silicon Integrated Mach-Zehnder Interferometer Waveguide for Biological and Chemical Sensing. *Opt Express* (2013) 21(17): 19488–19497. doi:10.1364/OE.21.019488
28. Stefano LD, Rotiroti L, Rea I, Moretti L, Di Francia G, Massera E, et al. Porous Silicon-Based Optical Biochips. *J Opt A, Pure Appl Opt* (2006) 8(7):S540–S544. doi:10.1088/1464-4258/8/7/s37
29. Rong G, Weiss SM. Biomolecule Size-dependent Sensitivity of Porous Silicon Sensors. *Phys Status Solidi A* (2009) 206(6):1365–1368. doi:10.1002/pssa.200881097
30. Rodriguez GA, Hu S, Weiss M. Porous Silicon Ring Resonator for Compact, High Sensitivity Biosensing Applications. *Opt Express* (2015) 23(6):7111–7119. doi:10.1364/oe.23.007111
31. Wongmanerod C, Zangooie S, Arwin H. Determination of Pore Size Distribution and Surface Area of Thin Porous Silicon Layers by Spectroscopic Ellipsometry. *Appl Surf Sci* (2001) 172(1-2):117–25. doi:10.1016/s0169-4332(00)00847-3

32. Sahu S, Ali J, Yupapin PP, Singh G. Porous Silicon Based Bragg-Grating Resonator for Refractive Index Biosensor. *Photonic Sens* (2018) 8(3):248–254. doi:10.1007/s13320-018-0459-z
33. Rajasekar R, Robinson S. Nano-Pressure and Temperature Sensor Based on Hexagonal Photonic Crystal Ring Resonator. *Plasmonics* (2019) 14:3–15. doi:10.1007/s11468-018-0771-x
34. Wang CT, Wang CY, Yu JH, Kuo IT, Tseng CW, Jau HC, et al. Highly Sensitive Optical Temperature Sensor Based on a SiN Micro-Ring Resonator with Liquid crystal Cladding. *Opt Express* (2016) 24(2):1002–1007. doi:10.1364/oe.24.001002
35. Zhang C, Kang G, Xiong Y, Xu T, Gu L, Gan X, et al. Photonic Thermometer with a Sub-millikelvin Resolution and Broad Temperature Range by Waveguide-Microring Fano Resonance. *Opt Express* (2020) 28(9): 12599–12608. doi:10.1364/oe.390966
36. Zhang X, Yang Y, Bai H, Wang J, Yan M, Xiao H, et al. Theoretical Aspects and Sensing Demonstrations of Cone-Shaped Inwall Capillary-Based Microsphere Resonators. *Photon Res* (2017) 5(5):516–520. doi:10.1364/prj.5.000516
37. Kim GD, Lee HS, Park CH, Lee SS, Lim BT, Bae HK, et al. Silicon Photonic Temperature Sensor Employing a Ring Resonator Manufactured Using a Standard CMOS Process. *Opt Express* (2010) 18(21):22215–22221. doi:10.1364/oe.18.022215
38. Ma T, Yuan J, Sun L, Kang Z, Yan B, Sang X, et al. Simultaneous Measurement of the Refractive Index and Temperature Based on Microdisk Resonator with Two Whispering-Gallery Modes. *IEEE Photon J* (2017) 9(1):1–13. art. no. 6800913. doi:10.1109/jphot.2017.2648259
39. Jabin MA, Ahmed K, Rana MJ, Paul BK, Islam M, Vigneswaran D, et al. Surface Plasmon Resonance Based Titanium Coated Biosensor for Cancer Cell Detection. *IEEE Photon J* (2019) 11(4):1–10. art. no. 3700110. doi:10.1109/jphot.2019.2924825

Conflict of Interest: The authors declare that the research was conducted in the absence of any commercial or financial relationships that could be construed as a potential conflict of interest.

Publisher's Note: All claims expressed in this article are solely those of the authors and do not necessarily represent those of their affiliated organizations, or those of the publisher, the editors, and the reviewers. Any product that may be evaluated in this article, or claim that may be made by its manufacturer, is not guaranteed or endorsed by the publisher.